PHYSICAL REVIEW D **90,** 074012 (2014)

Left-right spin asymmetry in $\ell N^{\uparrow} \to hX$

Leonard Gamberg,[1,*] Zhong-Bo Kang,[2,†] Andreas Metz,[3,‡] Daniel Pitonyak,[4,§] and Alexei Prokudin[5,‖]

[1]*Division of Science, Penn State Berks, Reading, Pennsylvania 19610, USA*
[2]*Los Alamos National Laboratory, Theoretical Division, Los Alamos, New Mexico 87545, USA*
[3]*Department of Physics, Barton Hall, Temple University, Philadelphia, Pennsylvania 19122, USA*
[4]*RIKEN BNL Research Center, Brookhaven National Laboratory, Upton, New York 11973, USA*
[5]*Jefferson Lab, 12000 Jefferson Avenue, Newport News, Virginia 23606, USA*

(Received 30 July 2014; published 9 October 2014)

We consider the inclusive production of hadrons in lepton-nucleon scattering. For a transversely polarized nucleon this reaction shows a left-right azimuthal asymmetry, which we compute in twist-3 collinear factorization at leading order in perturbation theory. All nonperturbative parton correlators of the calculation are fixed through information from other hard processes. Our results for the left-right asymmetry agree in sign with recent data for charged pion production from the HERMES Collaboration and from Jefferson Lab. However, the magnitude of the computed asymmetries tends to be larger than the data. Potential reasons for this outcome are identified. We also give predictions for future experiments and highlight in particular the unique opportunities at an electron ion collider.

DOI: 10.1103/PhysRevD.90.074012 PACS numbers: 13.88.+e, 13.85.Ni, 13.60.−r, 13.85.Qk

I. INTRODUCTION

In the present work we study inclusive production of hadrons in lepton-nucleon scattering, $\ell N \to hX$. If the transverse momentum $P_{h\perp}$ of the final state hadron is sufficiently large, this process may be treated in perturbative quantum chromodynamics (QCD) and, therefore, can provide additional information about the parton structure of the nucleon. Our focus here is on the left-right azimuthal asymmetry that can be defined if the nucleon is transversely polarized. This asymmetry is similar to the transverse single-spin asymmetry A_N which has already been studied extensively in hadronic collisions like $p^{\uparrow} p \to hX$—see Refs. [1–31] for related experimental and theoretical work. Recently, the HERMES Collaboration [32] and the Jefferson Lab Hall A Collaboration [33] reported the first ever measurements of A_N in lepton-nucleon scattering. In general, one may expect that A_N in this reaction could give new insight into the underlying mechanism of A_N in hadronic collisions which is the subject of longstanding discussions.

We compute A_N in collinear twist-3 factorization where it has two main components: First, a twist-3 effect originates from the transversely polarized nucleon. In that case the key nonperturbative entity is the so-called Qiu-Sterman (QS) function [12,13]—a specific quark-gluon-quark correlator that has an intimate connection with the transverse momentum dependent (TMD) Sivers function [34,35]. In a closely related previous work we have shown how the QS function can be studied through measuring A_N for the process $\ell p^{\uparrow} \to \text{jet}X$ [36]. Second, a twist-3 effect also arises from parton fragmentation. This contribution can be expressed by means of two independent fragmentation correlators [30,37,38], one of which is related to the Collins fragmentation function [39]. A first attempt to get a complete result for A_N in $\ell p^{\uparrow} \to hX$ in the collinear twist-3 approach can be found in [40]. Note that the same observable has also been computed in the so-called generalized parton model (GPM), which uses TMD parton correlation functions [41–43].

We fix all the nonperturbative parts of the analytical result for A_N through available information from other hard scattering processes. In particular, we take into account important input for the fragmentation correlators from a recent analysis of A_N in $p^{\uparrow} p \to \pi X$ [31]. Our calculation agrees in sign with the data from HERMES [32] and from Jefferson Lab [33]. On the other hand, the results tend to be larger than the data. As we discuss below in more detail, the most important reasons for this outcome could be the underestimated error of our calculation, and the impact from higher order corrections. Such corrections can be expected to be very large for $\ell N \to hX$ in the kinematical region of the presently available data. We therefore emphasize the need for a next-to-leading order (NLO) calculation of A_N in order to explore to what extent this observable is theoretically under control. We also stress the importance of new experiments, in particular at a future electron ion collider (EIC) [44–46]. With such a facility one could extend the measurements to (much) higher values of $P_{h\perp}$ where the perturbative expansion converges better. Moreover, an EIC would allow one for the first time to explore the forward region of the nucleon in a lepton-nucleon reaction. Note that it is precisely this forward

*lpg10@psu.edu
†zkang@lanl.gov
‡metza@temple.edu
§dpitonyak@quark.phy.bnl.gov
‖prokudin@jlab.org

region of the polarized nucleon where strikingly large asymmetries A_N have been observed in $p^\uparrow p \to hX$ [1,3,5–8].

Our paper is organized as follows. In Sec. II we present some details of the kinematics for $\ell N \to hX$ as well as our analytical results. The numerical results are given in Sec. III. They include the comparison to existing data and predictions for future experiments. In Sec. III we also briefly compare our approach with the GPM. The paper is summarized in Sec. IV.

II. KINEMATICS AND ANALYTICAL RESULTS

Here we discuss some details of the kinematics and present the tree-level results for the unpolarized and the spin-dependent cross section entering the definition of A_N. For the process under consideration

$$\ell(l) + N(P, S_P) \to h(P_h) + X, \tag{1}$$

l, P, and P_h denote the momentum of the lepton, nucleon, and produced hadron, respectively, and S_P is the spin vector of the nucleon. We use the momenta of the particles to fix a coordinate system according to $\hat{e}_z = \hat{P} = -\hat{l}$, $\hat{e}_x = \hat{P}_{h\perp}$, and $\hat{e}_y = \hat{e}_z \times \hat{e}_x$. The Mandelstam variables for the scattering process are defined by

$$S = (l+P)^2, \qquad T = (P - P_h)^2, \qquad U = (l - P_h)^2, \tag{2}$$

while at the corresponding partonic level one has

$$\hat{s} = (l+k)^2 = xS, \qquad \hat{t} = (k-p)^2 = \frac{xT}{z},$$
$$\hat{u} = (l-p)^2 = \frac{U}{z}, \tag{3}$$

with k characterizing the momentum of the active quark in the nucleon, and p the momentum of the fragmenting quark. Neglecting parton transverse momenta one has $k = xP$ and $p = P_h/z$.

For the unpolarized lepton-nucleon collisions, the differential cross section at leading order (LO) is given by [36]

$$P_h^0 \frac{d\sigma_{UU}}{d^3\vec{P}_h} = \frac{2\alpha_{\rm em}^2}{S} \sum_q e_q^2 \int_{z_{\min}}^1 \frac{dz}{z^2} \frac{1}{S + T/z} \times \frac{1}{x} f_1^q(x) D_1^{h/q}(z) \left[\frac{\hat{s}^2 + \hat{u}^2}{\hat{t}^2}\right], \tag{4}$$

where f_1^q is the unpolarized quark distribution, and $D_1^{h/q}$ is the unpolarized fragmentation function. Here $z_{\min} = -(T+U)/S$, and x can be determined from the on-shell condition $\hat{s} + \hat{t} + \hat{u} = 0$ in our LO formula as

$$x = -(U/z)/(S + T/z). \tag{5}$$

We now turn to the spin-dependent cross section for the process $\ell N^\uparrow \to hX$, that is, an unpolarized lepton scattering off a transversely polarized nucleon. We work in the collinear factorization framework, in which this cross section is a twist-3 observable. The twist-3 effect can either come from the side of the parton distribution in the transversely polarized nucleon [12], or from the side of the parton fragmentation into the final-state hadron [28,30,37]. Calculations for such a twist-3 observable in collinear factorization have become standard, and details can be found in the literature—see, e.g., Refs. [12–15,22–24,28,30,37,38,47–54]. In particular, we refer to [30] where the fragmentation contribution to A_N for $p^\uparrow p \to hX$ has been computed. Here we only write down the final expression

$$P_h^0 \frac{d\sigma_{UT}}{d^3\vec{P}_h} = -\frac{8\alpha_{\rm em}^2}{S} \varepsilon_{\perp\mu\nu} S_{P\perp}^\mu P_{h\perp}^\nu \sum_q e_q^2 \int_{z_{\min}}^1 \frac{dz}{z^3} \frac{1}{S + T/z} \frac{1}{x} \left\{ -\frac{\pi M}{\hat{u}} D_1^{h/q}(z) \left(F_{FT}^q(x,x) - x \frac{dF_{FT}^q(x,x)}{dx} \right) \left[\frac{\hat{s}(\hat{s}^2 + \hat{u}^2)}{2\hat{t}^3}\right] \right.$$
$$+ \frac{M_h}{-x\hat{u} - \hat{t}} h_1^q(x) \left\{ \left(\hat{H}^{h/q}(z) - z \frac{d\hat{H}^{h/q}(z)}{dz} \right) \left[\frac{(1-x)\hat{s}\,\hat{u}}{\hat{t}^2}\right] \right.$$
$$\left. \left. + \frac{1}{z} H^{h/q}(z) \left[\frac{\hat{s}(\hat{s}^2 + (x-1)\hat{u}^2)}{\hat{t}^3}\right] + 2z^2 \int_z^\infty \frac{dz_1}{z_1^2} \frac{1}{\frac{1}{z} - \frac{1}{z_1}} \hat{H}_{FU}^{h/q,\Im}(z, z_1) \left[\frac{x\hat{s}^2\hat{u}}{\xi_z \hat{t}^3}\right] \right\} \right\}, \tag{6}$$

where we use the convention $\varepsilon_\perp^{12} \equiv \varepsilon^{-+12} = 1$, and $\xi_z = z/z_g$ with $1/z_g = (1/z - 1/z_1)$. For the electromagnetic interaction we used both Feynman gauge and a light-cone gauge. In either case we obtained identical results which can be considered a nontrivial cross check of the calculation. At the operator level and in a parton model analysis, the QS function F_{FT}^q [12,13] can be related to the first $k_\perp$ moment of the Sivers function $f_{1T}^{\perp q}$ [16,55],

$$\pi F_{FT}^q(x,x) = \int d^2\vec{k}_\perp \frac{\vec{k}_\perp^2}{2M^2} f_{1T}^{\perp q}(x, \vec{k}_\perp^2)\Big|_{\rm SIDIS}, \tag{7}$$

where the subscript "SIDIS" indicates the Sivers function probed in semi-inclusive deep-inelastic scattering. More information about the relation between the QS function and the Sivers effect when taking into account evolution can be

found in [56,57]. The function $\hat{H}^{h/q}$ has the following relation to the Collins function $H_1^{\perp h/q}$ [28,30,37]:

$$\hat{H}^{h/q}(z) = z^2 \int d^2\vec{p}_\perp \frac{\vec{p}_\perp^{\,2}}{2M_h^2} H_1^{\perp h/q}(z, z^2\vec{p}_\perp^{\,2}). \quad (8)$$

Our definitions for both $f_{1T}^{\perp q}$ and $H_1^{\perp h/q}$ follow the so-called Trento convention [58]. On the fragmentation side σ_{UT} contains two additional twist-3 terms. Those depend on the two-parton correlator $H^{h/q}$ and the (imaginary part of the) 3-parton correlator $\hat{H}_{FU}^{h/q}$. The underlying dynamics for these functions may be similar to the one for the Collins effect, and it turns out in fact that $\hat{H}^{h/q}$, $H^{h/q}$, and $\hat{H}_{FU}^{h/q,\Im}$ are not independent of each other but satisfy the relation [30]

$$H^{h/q}(z) = -2z\hat{H}^{h/q}(z) + 2z^3 \int_z^\infty \frac{dz_1}{z_1^2} \frac{1}{\frac{1}{z} - \frac{1}{z_1}} \hat{H}_{FU}^{h/q,\Im}(z, z_1). \quad (9)$$

Since both the Sivers function $f_{1T}^{\perp q}$ and the Collins function $H_1^{\perp h/q}$ have been extracted from experimental data [59–69], one has information for the twist-3 correlators $F_{FT}^q(x,x)$ and $\hat{H}^{h/q}(z)$ through Eqs. (7) and (8). In order to estimate the contributions from the different terms in Eq. (6), the only unknown piece is the 3-parton correlator $\hat{H}_{FU}^{h/q,\Im}$ after taking advantage of the relation in Eq. (9). In Ref. [31] it was argued that the fragmentation functions $H^{h/q}$ and $\hat{H}_{FU}^{h/q,\Im}$ could be the main source of the left-right asymmetry A_N for $p^\uparrow p \to \pi X$. In our numerical estimates in the next section we will use the fitted parametrization for $\hat{H}_{FU}^{h/q,\Im}$ from [31]. In principle through the process under consideration one can learn more about the fragmentation functions entering twist-3 calculations, which in turn could help one to better understand A_N in proton-proton collisions where the same functions show up. In practice, however, this may be difficult due to potentially large NLO radiative corrections for $\ell N \to hX$ [36,70]. Below we will return to this point.

III. NUMERICAL ESTIMATES

In this section, we will estimate A_N based on the LO formulas in Eqs. (4) and (6). We will study in detail the contributions from the soft-gluon pole term involving F_{FT}^q, and the fragmentation term involving $\hat{H}^{h/q}$, $H^{h/q}$, and $\hat{H}_{FU}^{h/q,\Im}$. Throughout we use the GRV98 unpolarized parton distributions [71] and the DSS unpolarized fragmentation functions [72]. We calculate the QS function F_{FT}^q using Eq. (7) and the Sivers function of Ref. [66] extracted from SIDIS data. The twist-3 fragmentation function $\hat{H}^{h/q}$ is calculated by using Eq. (8) and the Collins function extracted from SIDIS and e^+e^- data in Ref. [67]. The transversity function h_1^q is also taken from Ref. [67]. Note that antiquark transversity functions are neglected throughout since no information exists on their extraction. The function $\hat{H}_{FU}^{h/q,\Im}$ was fitted to data on A_N in pp scattering in Ref. [31], and we will use its parametrization, while $H^{h/q}$ is fixed through Eq. (9). For simplicity we assume that the twist-3 correlators follow the same DGLAP scale dependence as the twist-2 counterparts f_1^q or $D_1^{h/q}$. For more information on the proper evolution of 3-parton correlators we refer to [73–82].

A. Single spin asymmetry

In order to compare our calculation to the spin asymmetry measured by the HERMES Collaboration [32] we first need to carefully consider the conventions. In Ref. [32] the transverse SSA is denoted by $A_{UT}^{\sin\Psi}$ and defined through

$$d\sigma = d\sigma_{UU}(1 + S_{P\perp} A_{UT}^{\sin\Psi} \sin\Psi). \quad (10)$$

Here the $\sin\Psi$ azimuthal dependence is determined from the vector product $\vec{S}_{P\perp} \cdot (\vec{P}_h \times \vec{l})$ where, as stated above, $\vec{S}_{P\perp}$ is the (transverse) spin vector of the target, and $\vec{l}$ and $\vec{P}_h$ are the three-momenta of the incident lepton and of the final-state hadron, respectively. The asymmetry is defined in the lepton-nucleon center-of-mass frame such that the lepton moves in the $+z$ direction, while the transversely polarized nucleon moves along the $-z$ direction. While in the pp case the transversely polarized nucleon typically defines the $+z$ direction, it is important to realize that the definition of $A_{UT}^{\sin\Psi}$ fully agrees with the one for A_N used for pp collisions [1–3,5–9]. Note also that in the HERMES convention positive Feynman x (which we denote by x_F^H) corresponds to hadrons going in the direction of the lepton or backwards with respect to the target nucleon. This convention has the opposite sign compared to x_F used in the pp case [1–3,5–9], i.e., $x_F^H = -x_F$. With the coordinate system specified in Sec. II and the spin vector of the nucleon pointing in the $+y$ direction we have

$$\epsilon_{\perp\mu\nu} S_\perp^\mu P_{h\perp}^\nu = -P_{h\perp}, \quad x_F \equiv \frac{2P_{hz}}{\sqrt{S}} = -x_F^{\rm H}, \quad (11)$$

where $P_{h\perp} \equiv |\vec{P}_{h\perp}|$. The differential cross section can then be written as

$$P_h^0 \frac{d\sigma_{UT}}{d^3P_h} = \sqrt{4\frac{P_{h\perp}^2}{S} + x_F^2}\, \frac{d\sigma_{UT}}{dx_F d^2P_{h\perp}}, \quad (12)$$

and the spin asymmetry A_N is given by

$$A_N(x_F, P_{h\perp}) \equiv \frac{\sqrt{4\frac{P_{h\perp}^2}{S} + x_F^2}\, \frac{d\sigma_{UT}}{dx_F d^2P_{h\perp}}}{\sqrt{4\frac{P_{h\perp}^2}{S} + x_F^2}\, \frac{d\sigma_{UU}}{dx_F d^2P_{h\perp}}} = A_{UT}^{\sin\Psi}(-x_F^H, P_{h\perp}). \quad (13)$$

The Mandelstam variables T and U can be expressed in terms of x_F and $P_{h\perp}$ as

$$T = -\sqrt{S}\sqrt{P_{h\perp}^2 + x_F^2\frac{S}{4}} + x_F\frac{S}{2},$$
$$U = -\sqrt{S}\sqrt{P_{h\perp}^2 + x_F^2\frac{S}{4}} - x_F\frac{S}{2}. \quad (14)$$

These relations will help us to better understand the kinematical regions that are covered in the integration in Eqs. (4) and (6). In particular, let us consider a situation $S \gg P_{h\perp}^2$ and $x_F \to -1$ ($x_F^{\rm H} \to 1$). It is easy to see that in this case $T \to -S$, $U \to 0$. If $x_F \to 1$ ($x_F^{\rm H} \to -1$), we have $T \to 0$, $U \to -S$. We may conclude from Eq. (5) that for $x_F \to 1$ ($x_F^{\rm H} \to -1$) the region of x will be concentrated around 1, i.e., the large-x region, and for $x_F \to -1$ ($x_F^{\rm H} \to 1$) x will be in the region [0, 1], i.e., relatively small-x region. On the other hand, the region explored in z spans from $z_{\rm min} = -(T+U)/S$ to 1 and is obviously symmetric with respect to $x_F \leftrightarrow -x_F$. The region of z will shrink to 1 for both $x_F \to \pm 1$.

It is good to discuss the uncertainties in our formalism, which mainly come from F_{FT}^q, h_1^q, $\hat{H}^{h/q}$, and $\hat{H}_{FU}^{h/q,\Im}$. The errors of F_{FT}^q, h_1^q, and $\hat{H}^{h/q}$ are propagated from the errors of TMD distributions which were extracted in [66,67]. The errors of these TMD distributions were estimated in [66,67] using the method described in Appendix A of [66]. Let us briefly recall this method: In order to calculate the errors we generate randomly 200 sets of parameters for each of the distributions considered such that each of the set gives χ^2 which is within $\Delta\chi^2$ (chosen to correspond to 95% of confidence level) above the minimum $\chi^2_{\rm min}$ reached by global minimization on the corresponding experimental data set. In order to calculate the errors on the observables, we then compute these observables using all 200 sets and find a minimum and maximum for each point. By doing so we plot an error band for all curves in this paper: in other words, the uncertainty band on all the plots in the rest of the paper contains only the errors of these TMD functions. Notice that through this procedure we have a joint estimation of errors for transversity and Collins fragmentation function (FF) simultaneously as they enter into observables together. It is natural to expect that uncertainties of corresponding functions grow in the region where the experimental data are not available, for example for the Sivers function and transversity at large x (or negative x_F^H). From this simple analysis, we can conclude that in the region of $x_F \to 1$ ($x_F^H \to -1$) our calculations will have the largest uncertainties based on the uncertainties in the TMD functions. This is because this x-range probes the as yet unexplored regions in SIDIS of large $x, z \to 1$. On the other hand in the regime $x_F \to -1$ ($x_F^H \to 1$) we expect to have smaller uncertainties based on the uncertainties in the TMD functions as far as this region of x corresponds to the kinematical regime already explored in SIDIS. In order to corroborate these findings we also present the numerical computation of x and z as a function of x_F^H in the case of HERMES kinematics at $\sqrt{S} = 7.25$ GeV for $P_{h\perp} = 1$ GeV in Fig. 1. One can see that, in particular, in the region of positive x_F^H (negative x_F), the region of x indeed corresponds to the region explored by SIDIS data. Note in the cross section for ℓp that z is integrated over while x is fixed once z is known (or vice versa). But in the case of pp collisions, once z is known, only a minimum x-value $x_{\rm min}$ is fixed, with an x integration evaluated from $x_{\rm min}$ to 1.

Nevertheless, one must keep in mind that the function $\hat{H}_{FU}^{h/q,\Im}$ was fitted to experimental data in proton-proton scattering which are in the large positive x_F range (i.e., large negative x_F^H region) not explored by inclusive hadron production in lepton-proton scattering at HERMES. Error bands for these functions were not computed in Ref. [31]. However, one might speculate in the region of $x_F^H > 0$ ($x_F < 0$), where limited information from pp collisions exists and none is available for charged pions, there are large errors. Without the uncertainty of $\hat{H}_{FU}^{h/q,\Im}$ included, the error bands in the plots are thus underestimated in this $x_F^H > 0$ region. In addition, even in the $x_F > 0$ region covered by the pp data, one has uncertainties in $\hat{H}_{FU}^{h/q,\Im}$ due to uncertainties in the Sivers, Collins, and transversity functions that were used as inputs in the analysis of Ref. [31]. This is readily seen in the different fits obtained in Ref. [31] when using two different extractions of the

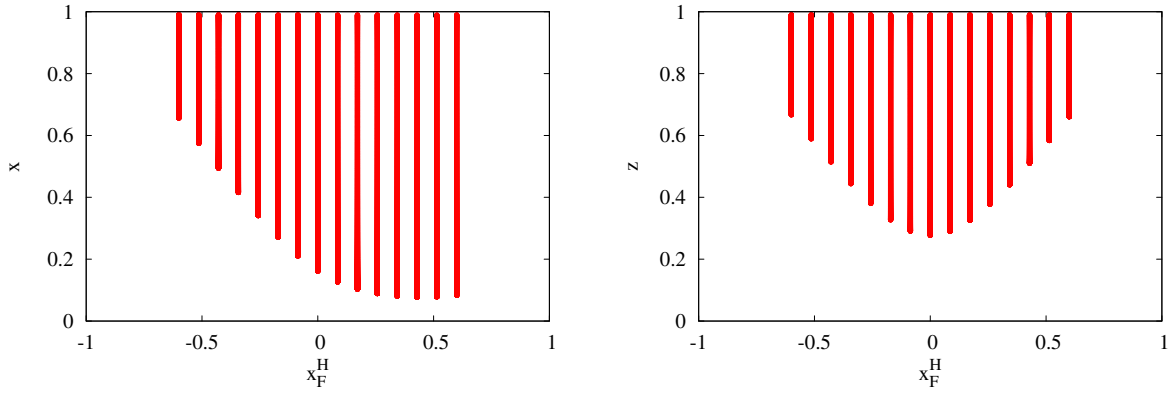

FIG. 1 (color online). Region covered in x (left panel) and in z (right panel) as a function of $x_F^{\rm H}$.

Sivers functions. Since $z_{\min}$ increases as x_F increases, this implies large uncertainties in $\hat{H}_{FU}^{h/q,\Im}$ in the large-z region covered by the HERMES data (see Fig. 1). There are also uncertainties in $\hat{H}_{FU}^{h/q,\Im}$ related to the neglect of soft-fermion poles in the pp reaction, which may play some role in A_N for that process [24]. In any case, a complete analysis of both ℓp and pp asymmetry data within the factorization formalisms (with enough accuracy in theoretical calculations) should better constrain $\hat{H}_{FU}^{h/q,\Im}$, and in turn help to more thoroughly understand this fragmentation mechanism that could underlie single-spin asymmetries in proton-proton collisions [31].

B. Comparison with the experimental data

In the following we will plot $A_N(-x_F, P_{h\perp}) = A_{UT}^{\sin\Psi}(x_F^H, P_{h\perp})$ as a function of x_F^H and $P_{h\perp}$. It is important to realize that for the process at hand, $\ell N \to hX$, only the hadron transverse momentum $P_{h\perp}$ can serve as the hard scale. We thus choose the renormalization scale for both parton distributions and fragmentation functions as $P_{h\perp}$, which has to satisfy $P_{h\perp} \gg \Lambda_{\rm QCD}$ to ensure the use of collinear factorization formalism. With this in mind, we therefore only compare with the HERMES data in Ref. [32] with $P_{h\perp} \geq 1$ GeV. We note that almost all of this data is from quasireal photoproduction (i.e., $Q^2 \sim 0$ GeV^2). We will address later how this could affect the comparison between theory and experiment.

In Fig. 2 we plot A_N as a function of $x_F^{\rm H}$ for π^+ and π^- production with $1 < P_{h\perp} < 2.2$ GeV ($\langle P_{h\perp}\rangle \simeq 1$ GeV) for lepton-proton collisions at HERMES energy $\sqrt{S} = 7.25$ GeV [32]. For π^+ the contribution coming from F_{FT}^q related to the Sivers effect is positive for all x_F. The contribution from $\hat{H}^{h/q}$ is of opposite sign and smaller in absolute value than that from F_{FT}^q. The contribution from $H^{h/q}$ is positive and that from $\hat{H}_{FU}^{h/q,\Im}$ is negative, and their sum is similar in absolute value to the contribution from $\hat{H}^{h/q}$. In fact those three contributions almost cancel each other leaving a nearly vanishing fragmentation piece. The resulting asymmetry is close to the contribution from F_{FT}^q and is larger than the experimental data, as clearly seen in the figure. The experimental data are around 5% and our computations result in a positive asymmetry of about 15%.

On the other hand, for π^- the contribution coming from F_{FT}^q is negative for positive $x_F^{\rm H}$ and the contribution from $\hat{H}^{h/q}$ is of opposite sign and comparable to that from F_{FT}^q. The contribution for positive x_F^H from $H^{h/q}$ is negative and from $\hat{H}_{FU}^{h/q,\Im}$ is positive. The fragmentation piece contributes roughly the same as F_{FT}^q does at moderate x_F^H but begins to dominate at smaller (and negative) x_F^H. Our computations result in a negative asymmetry of about -15% in the positive $x_F^{\rm H}$ region whereas the experimental data are close to zero.

In Fig. 3 we plot A_N as function of $P_{h\perp}$ for lepton-proton collisions at HERMES energy $\sqrt{S} = 7.25$ GeV [32]. The general trends for all contributions are similar to those for the x_F dependence shown in Fig. 2 and described above. One may sense, though, that, as could have been expected, our LO calculation is doing better towards larger values of $P_{h\perp}$.

Before we proceed, let us elaborate more on the contribution due to the 3-parton correlator $\hat{H}_{FU}^{h/q,\Im}$. According to Ref. [31], $\hat{H}_{FU}^{h/q,\Im}$, in particular through its contribution to $H^{h/q}$ via Eq. (9), might play a critical role for the description of A_N in $p^\uparrow p \to hX$ in the collinear twist-3 approach. In Fig. 4 we present our computations for A_N when $\hat{H}_{FU}^{h/q,\Im}$ is switched off. [Note that setting $H^{h/q}$ and $\hat{H}_{FU}^{h/q,\Im}$ to zero simultaneously would also imply $\hat{H}^{h/q} = 0$ due to the relation in Eq. (9).] Comparing with Fig. 2 one observes that $A_N^{\pi^+}$ does not change very much. On the other hand, the influence on $A_N^{\pi^-}$ is quite significant. In the x_F^H region of the HERMES data, the magnitude of the

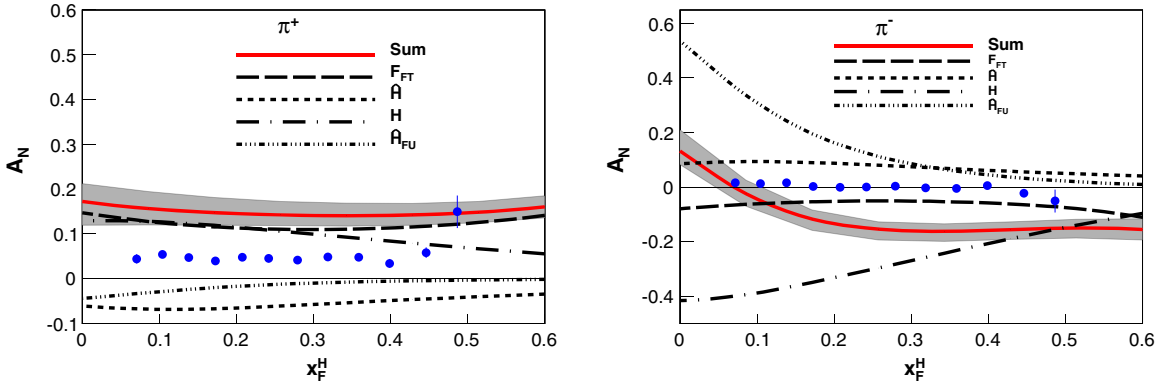

FIG. 2 (color online). A_N as a function of x_F^H for π^+ (left panel) and π^- (right panel) production at $P_{h\perp} = 1$ GeV for lepton-proton collisions at $\sqrt{S} = 7.25$ GeV. The data are from Ref. [32]. The solid line corresponds to the sum of all contributions. The F_{FT}^q contribution is the dashed line, the $\hat{H}^{h/q}$ contribution is the dotted line, the $H^{h/q}$ contribution is the dot-dashed line, and the $\hat{H}_{FU}^{h/q}$ contribution is the 3-dotted-dashed line. The error band comes from uncertainties in the Sivers, Collins, and transversity functions estimated in Refs. [66,67]. Note that positive $x_F^{\rm H}$ corresponds to pions in the backward direction with respect to the target proton.

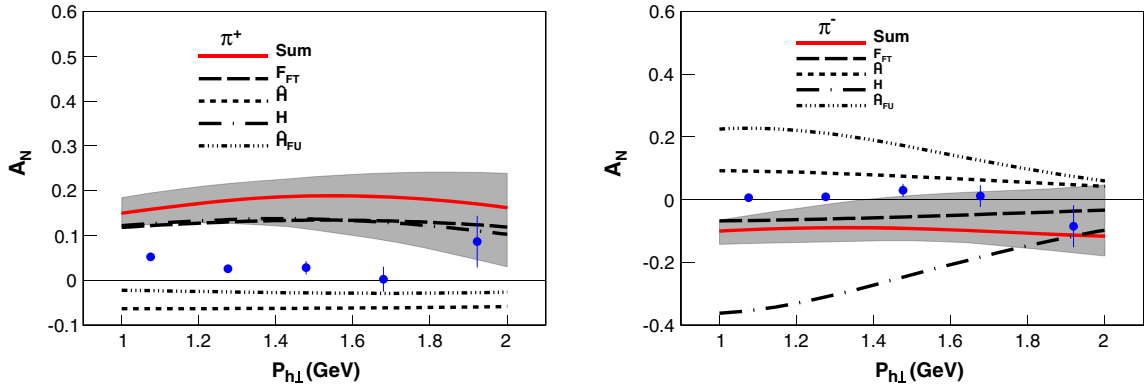

FIG. 3 (color online). A_N as function of $P_{h\perp}$ for π^+ (left panel) and π^- (right panel) production for lepton-proton collisions at $0.1 < x_F^{\mathrm{H}} < 0.2$ ($\langle x_F^{\mathrm{H}} \rangle \simeq 0.15$) and $\sqrt{S} = 7.25$ GeV. The data are from Ref. [32]. The description of lines is the same as in Fig 2.

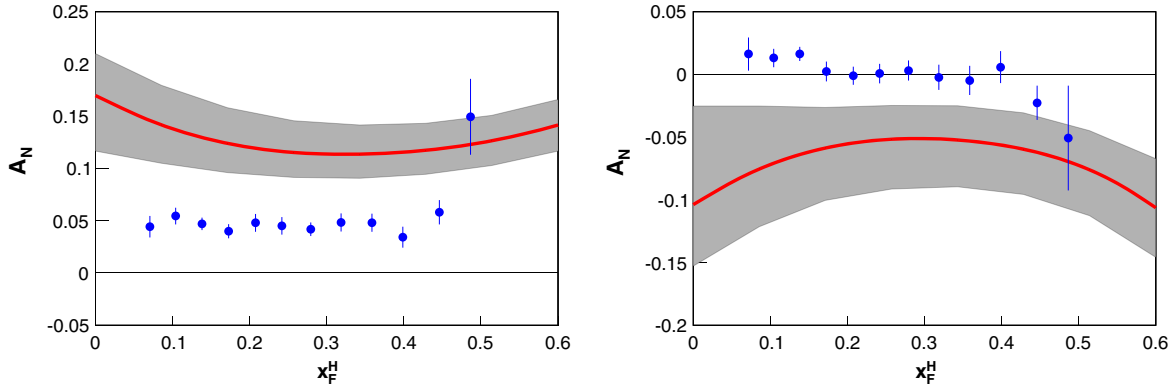

FIG. 4 (color online). A_N as a function of x_F^H for π^+ (left panel) and π^- (right panel) production at $P_{h\perp} = 1$ GeV and $\sqrt{S} = 7.25$ GeV. The data are from Ref. [32]. The solid line corresponds to sum of all contributions with $\hat{H}_{FU}^{h/q,\Im} = 0$.

asymmetry is reduced by about a factor 2. The influence of switching off $\hat{H}_{FU}^{h/q,\Im}$ is most dramatic in the region of relatively small x_F^H (in fact also negative x_F^H as we have checked) where $A_N^{\pi^-}$ even changes sign. In that region an EIC could provide unique information as we discuss in more detail in Sec. III C.

HERMES also explored several subsets of data where the outgoing lepton was detected and photon virtuality $Q^2 > 1$ GeV^2 was guaranteed, which were referred as "DIS" subsets [32]. This subset was divided into two regions of z: $0.2 < z < 0.7$ ($\langle x_F^{\mathrm{H}} \rangle \approx 0.2$) and $z > 0.7$ ($\langle x_F^{\mathrm{H}} \rangle \approx 0.27$). Even though strictly speaking these data sets correspond to semi-inclusive rather then fully inclusive hadron production, we will nevertheless compare our calculations with these measurements. In Fig. 5 we plot A_N for π^+ and π^- production as a function of $P_{h\perp}$ for

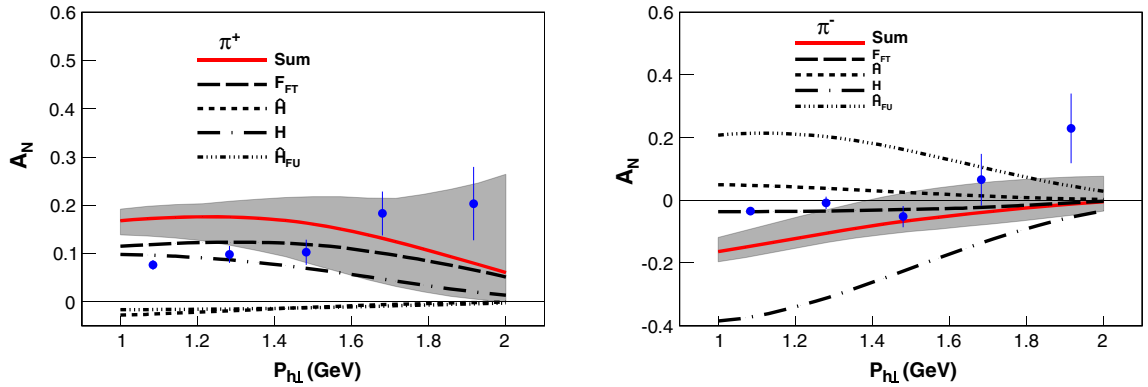

FIG. 5 (color online). A_N as function of $P_{h\perp}$ for π^+ (left panel) and π^- (right panel) production at $\langle x_F^{\mathrm{H}} \rangle \approx 0.2$ ($0.2 < z < 0.7$) and $\sqrt{S} = 7.25$ GeV for the "DIS" subset of the data from Ref. [32]. The description of lines is the same as in Fig. 2.

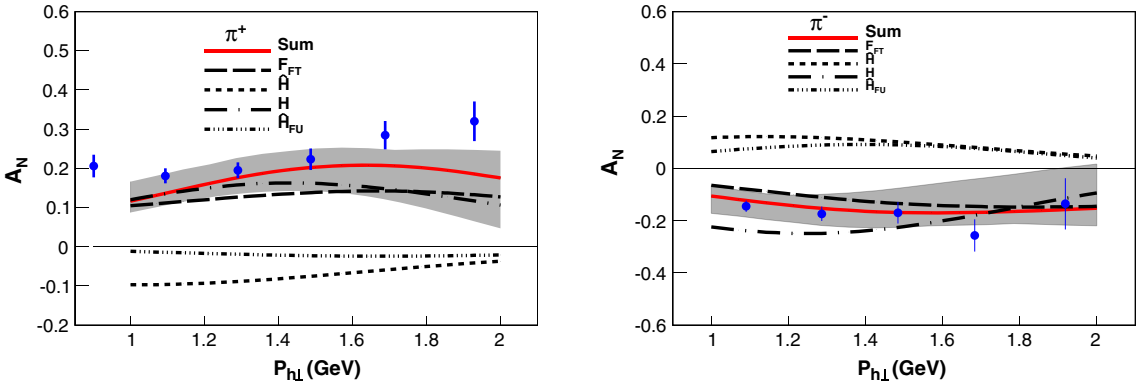

FIG. 6 (color online). A_N as function of $P_{h\perp}$ for π^+ (left panel) and π^- (right panel) production at $\langle x_F^{\mathrm{H}}\rangle \approx 0.27$ $(z > 0.7)$ and $\sqrt{S} = 7.25$ GeV for the "DIS" subset of the data from Ref. [32]. The description of lines is the same as in Fig. 2.

$0.2 < z < 0.7$. One can see that for π^+ the F_{FT}^q and $H^{h/q}$ terms dominate, while the $\hat{H}_{FU}^{h/q,\Im}$ and $\hat{H}^{h/q}$ pieces are negligible. For π^- the contribution from F_{FT}^q becomes smaller, and the $H^{h/q}$ and $\hat{H}_{FU}^{h/q,\Im}$ terms are sizable (with opposite sign) but decrease quickly with increasing $P_{h\perp}$. A different pattern emerges for the $z > 0.7$ subset which we plot in Fig. 6. In this case, the contributions from $\hat{H}^{h/q}$ and $\hat{H}_{FU}^{h/q,\Im}$ almost cancel the contribution from $H^{h/q}$, and the asymmetry is close to the result for the contribution from F_{FT}^q. Overall, the theoretical curves are much closer to the experimental data for both π^+ and π^- production.

Jefferson Lab published data on $\ell N \to hX$ collected on a transversely polarized ^{3}He target [33]. The energy of the experiment is relatively low, such that the largest value of the transverse hadron momentum reached is $P_{h\perp} = 0.69$ GeV. Therefore, we cannot compare directly to the data. However, we can calculate the asymmetry in the region of larger $P_{h\perp}$. Note that the definition of the reference frame used in Ref. [33] for Jefferson Lab is such that

$$A_N(x_F, P_{h\perp}) = A_{UT}^{\sin\Psi}(-x_F^H, P_{h\perp}) = -A_N^{\mathrm{JLab}}(x_F, P_{h\perp}). \quad (15)$$

In Fig. 7 we plot $\pi^\pm$ production on the neutron at JLab 6 for $P_{h\perp} > 1$ GeV. In this case the contribution from the function $H^{h/q}$ almost exactly cancels the contributions from $\hat{H}^{h/q}$ and $\hat{H}_{FU}^{h/q,\Im}$, and the asymmetry is close to the result of the contribution F_{FT}^q. One can see from Fig. 7 that the sign of the asymmetry for both π^+ and π^- is consistent with our calculations, but for π^+ the trend of the result is much larger than the data. However, one has to keep in mind that especially for $A_N^{\pi^+}$ the uncertainties of the calculation are quite large where the dominant contribution comes from down quarks, whose Sivers function has rather large errors. Future results from JLab 12 [83] will allow us to have a better determination of down quark TMDs in the large x region.

Extra caution has to be taken when one looks at the comparison of our computations with the experimental data, which seems to show discrepancies. Such disagreements can have different sources. First, our numerics is based on LO analytical results only. However, higher order corrections to both the spin-independent and the spin-dependent cross sections can be expected to be very large

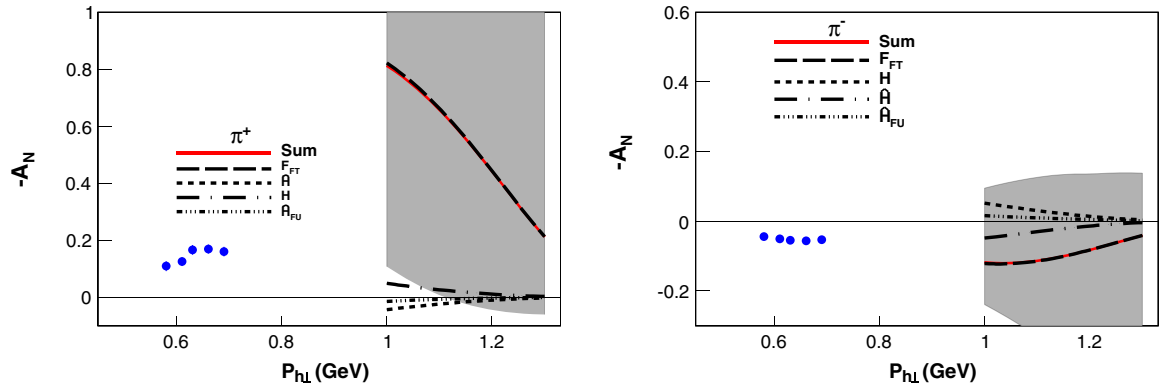

FIG. 7 (color online). $-A_N$ as function of $P_{h\perp}$ for π^+ (left panel) and π^- (right panel) production off a neutron at $\langle x_F\rangle \approx -0.26$ and $\sqrt{S} = 3.45$ GeV. The data are from Ref. [33]. The description of lines is the same as in Fig. 2.

for the process $\ell N \to hX$ [36,70], especially in the relatively low $P_{h\perp}$ region. This is actually already confirmed by the HERMES measurement [32], where almost all the data correspond to quasireal photoproduction, and even at the highest $P_{h\perp} \sim 2$ GeV only a very small fraction of the events satisfies $Q^2 > 1$ GeV^2. Since in collinear factorization quasireal photoproduction appears for the first time at NLO accuracy, the underlying mechanism of the majority of the data from HERMES (and Jefferson Lab) is not covered by a LO calculation. In order to obtain a more quantitative understanding of higher order corrections, it would be very useful to have absolute cross section measurements from HERMES and Jefferson Lab. At the same time, the NLO calculation has to be carried out in the future. Along these lines, the positive trend towards larger $P_{h\perp}$ values in Fig. 3 and, in particular, the relatively good agreement shown in Figs. 5 and 6, where one has data with $Q^2 > 1$ GeV^2, could indeed indicate that issues describing the HERMES data in Figs. 2 and 3 may be attributed to possibly large radiative corrections due to those data being at $Q^2 \sim 0$ GeV^2. Second, recall that the error bands are underestimated (see the discussion before Sec. III B), and may actually overlap the data once fully calculated.

C. Predictions

In this subsection, we show predictions for A_N in the kinematics relevant to several upcoming/planned experiments. A future EIC [44–46] with variable energy $\sqrt{S} =$ 50–100 GeV will be an ideal facility to study inclusive hadron production in $\ell p^\uparrow \to hX$. One reason is the possibility to measure at (much) larger values of $P_{h\perp}$ where the theory for this process should be under better control. We plot in Figs. 8 and 9 our predictions for π^0, π^+, π^- production at $\sqrt{S} = 63$ GeV and $P_{h\perp} = 3$ GeV. Note that for $p^\uparrow p \to \pi X$ in the forward region ($x_F > 0$) very large values for A_N have been observed. We find that a clearly nonzero A_N is predicted in this region. An EIC would be in a unique position to make a measurement for $x_F > 0$. As already alluded to in the discussion of Fig. 4, π^- production would be particularly interesting in order to study the underlying mechanism of A_N. One sees that setting $\hat{H}_{FU}^{h/q,\Im} = 0$, as in right panel of Fig. 9, leads to a negative A_N, opposite in sign for small to moderate x_F to the case where one keeps $\hat{H}_{FU}^{h/q,\Im}$ nonzero. Therefore, a measurement of A_N at $x_F > 0$ at an EIC can help constrain and test the extraction of this 3-parton fragmentation

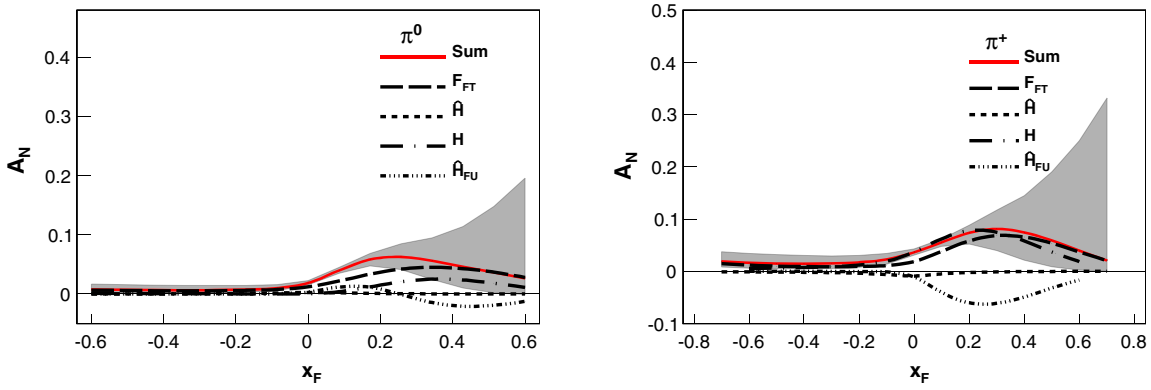

FIG. 8 (color online). Prediction for A_N as function of x_F for π^0 (left panel) and π^+ (right panel) production at $P_{h\perp} = 3$ GeV for EIC kinematics ($\sqrt{S} = 63$ GeV). The description of lines is the same as in Fig. 2.

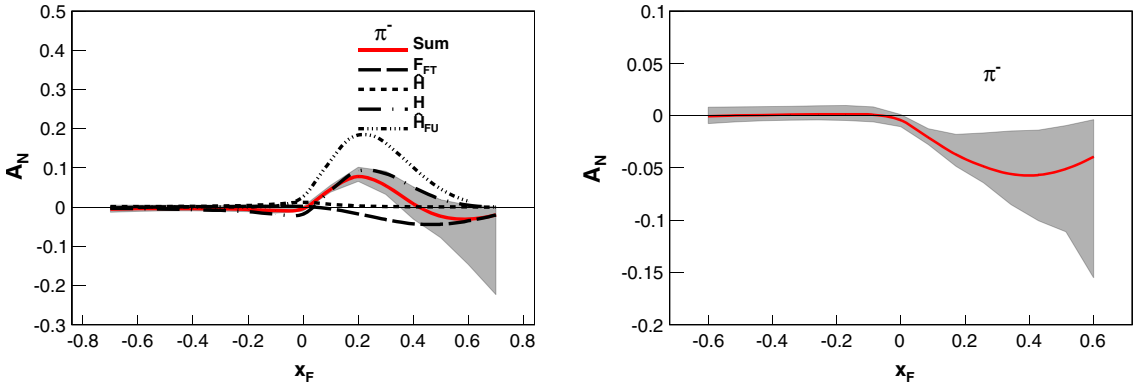

FIG. 9 (color online). Prediction for A_N as function of x_F for π^- (left panel) and π^- (right panel with $\hat{H}_{FU}^{h/q,\Im} = 0$) production at $P_{h\perp} = 3$ GeV for EIC kinematics ($\sqrt{S} = 63$ GeV). The description of lines is the same as in Fig. 2.

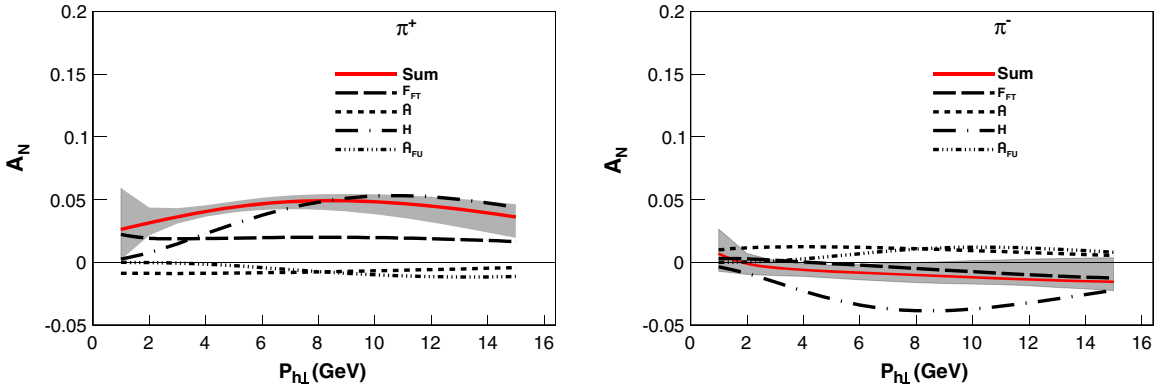

FIG. 10 (color online). Prediction for A_N as function of $P_{h\perp}$ for π^+ (left panel) and π^- (right panel) production at $x_F = 0$ for EIC kinematics ($\sqrt{S} = 63$ GeV). The description of lines is the same as in Fig. 2.

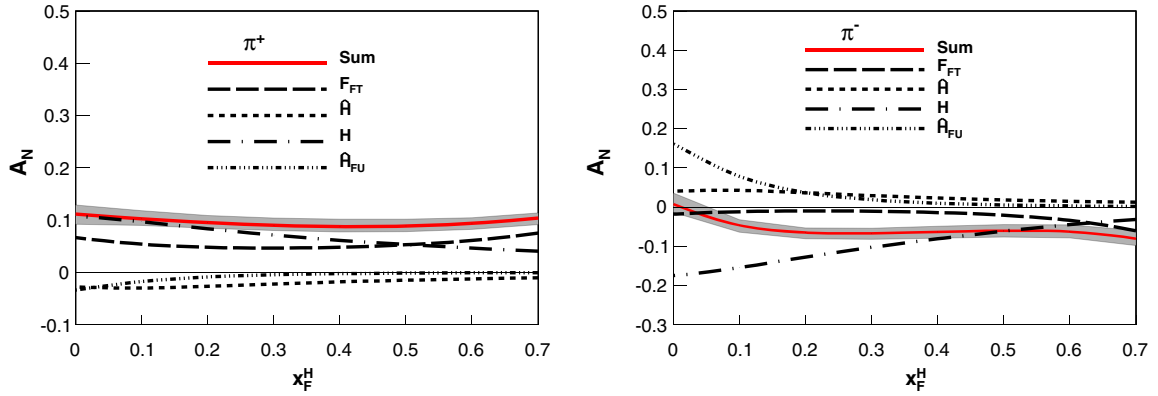

FIG. 11 (color online). Prediction for A_N as function of x_F^H for π^+ (left panel) and π^- (right panel) production at $P_{h\perp} = 2$ GeV for COMPASS kinematics ($\sqrt{S} = 17.3$ GeV). The description of lines is the same as in Fig. 2.

function performed in Ref. [31]. Predictions of A_N as a function of $P_{h\perp}$ at $x_F = 0$ for π^+, π^- production are shown in Fig. 10. One finds a rather flat $P_{h\perp}$ dependence like in the pp case [31]. In Fig. 11 we present our predictions for A_N as a function of x_F at $P_{h\perp} = 2$ GeV for both π^+ and π^- production for the COMPASS experiment at $\sqrt{S} = 17.3$ GeV. Similar predictions at $P_{h\perp} = 1$ GeV are shown in Fig. 12 for JLab 12 at $\sqrt{S} = 4.6$ GeV. It will be interesting to have experimental data on A_N from all these facilities in the future.

D. Comparison with the generalized parton model

Here we give a brief comparison between the collinear twist-3 approach and the GPM from both a conceptual and

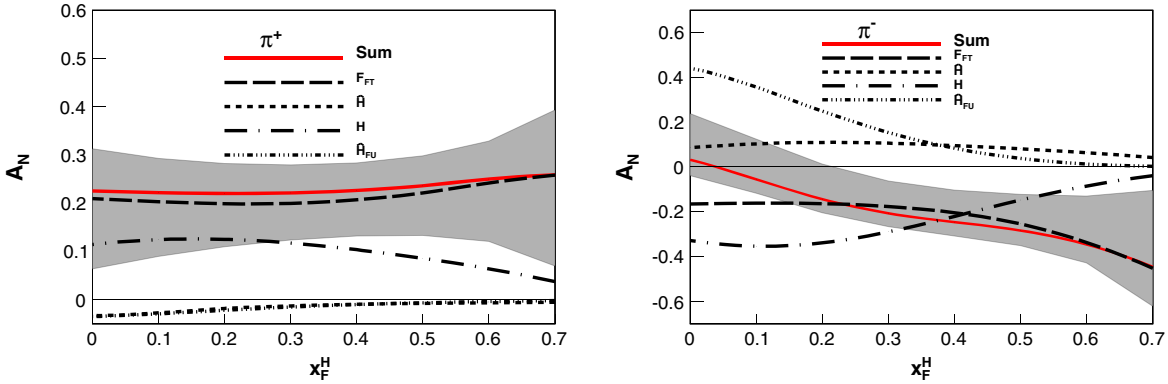

FIG. 12 (color online). Prediction for A_N as function of x_F^H for π^+ (left panel) and π^- (right panel) production at $P_{h\perp} = 1$ GeV for JLab 12 kinematics ($\sqrt{S} = 4.6$ GeV). The description of lines is the same as in Fig. 2.

a phenomenological point of view. The GPM has been applied to A_N for $\ell p^\uparrow \to hX$ [41–43] and for $p^\uparrow p \to hX$—see [17–21] and references therein. This model uses 2-parton correlation functions only, but consistently keeps the transverse parton momenta at all stages of the calculation. (This procedure may lead to a singularity for processes like $pp \to hX$ upon integrating over transverse momenta, which can however be avoided by introducing an integration cutoff [84–86].) In the case of twist-3 observables like A_N, not all leading power terms are covered by the GPM.[1] This holds for the twist-3 effect on the distribution side [88] and, in particular, also for the twist-3 fragmentation contribution [30]. As mentioned above, for the latter one has two independent fragmentation correlators [30], while in the GPM only the Collins function contributes. (At present, a detailed analytical comparison of the fragmentation contributions in the two approaches does not exist.) On the other hand, the GPM contains certain (kinematical) higher twist contributions and may also mimic effects of a collinear higher order calculation at leading twist. We note in passing that a recipe for incorporating in the GPM the process dependence of the Sivers effect [89] has been discussed in [88].

Let us now turn to the phenomenology of A_N for $\ell p^\uparrow \to hX$. The GPM predictions are closer to the HERMES data than what we found in the collinear twist-3 framework, where the best results in the GPM were obtained by exploiting somewhat older extractions of the Sivers function and the Collins function [60,64]—compare Fig. 1 and Fig. 2 in [43] with our Fig. 2. However, one again has to keep in mind the aforementioned underestimated error of the twist-3 calculation and the need for a NLO calculation. Moreover, due to large error bands, no conclusion could be drawn as to whether the Sivers or Collins effect can describe A_N in $p^\uparrow p \to \pi X$ within the GPM [20,21]. In this regard, a much more definite statement was made with the collinear twist-3 analysis performed in Ref. [31], i.e., that the fragmentation mechanism in that formalism can be the cause of the transverse single-spin asymmetries seen in pion production from proton-proton collisions.

We find that our results with $\hat{H}_{FU}^{h/q,\Im} = 0$ have the same signs and are close in magnitude to the curves labeled as SIDIS 2 in Figs. 1 and 2 of Ref. [43] for π^+ and π^- production, respectively. One may speculate then that an analytical relation between the GPM and twist-3 approaches (showing where the two formalisms agree and/or differ) is perhaps possible for this observable if one neglects the 3-parton FF. However, as already stated, no such rigorous derivation has been performed yet. Let us also mention that our prediction for $A_N^{\pi^+}$ for the EIC in Figs. 9 and 10 are comparable both in sign and size with those of Refs. [43,66] using GPM framework. On the other hand, our result for $A_N^{\pi^-}$ for the EIC is quite different from what one finds in the GPM [43,66]. Such a measurement might therefore allow one to discriminate between the phenomenology of the two approaches.

[1]A closely related discussion about the twist-3 so-called Cahn effect in SIDIS can be found in Ref. [87].

IV. SUMMARY

Within the collinear twist-3 factorization formalism, we derived LO results for the transverse single-spin asymmetry A_N for inclusive electroproduction of hadrons in lepton-nucleon collisions, $\ell N^\uparrow \to hX$. In such a process, A_N receives contributions from the QS function F_{FT}^q related to the quark Sivers function, from a twist-3 fragmentation function $\hat{H}^{h/q}$ related to the Collins function, and from two other twist-3 fragmentation functions $H^{h/q}$ and $\hat{H}_{FU}^{h/q,\Im}$. We provided numerical estimates for typical kinematics for experiments at HERMES [32] and at Jefferson Lab [33], and we compared our results with the HERMES data for $P_{h\perp} \geq 1$ GeV. We found that our theoretical estimates for A_N agree with the HERMES results in sign and roughly in shape, but in terms of magnitude they are typically above the data. We argued that at present such a discrepancy cannot be considered a failure of the collinear twist-3 formalism. We emphasized the need for computing the NLO corrections and assess its impact on A_N, especially in the region of lower transverse hadron momenta $P_{h\perp}$. Moreover, we explained why the error of our numerical calculations is underestimated. In this regard it will be important to better constrain the 3-parton fragmentation correlator $\hat{H}_{FU}^{h/q,\Im}$. On the experimental side, it would be very useful to have absolute cross section measurements from both HERMES and Jefferson Lab, which would help one to obtain a quantitative understanding of the role played by higher order corrections. We also presented predictions for A_N for Jefferson Lab 12, COMPASS, and a potential future electron ion collider. In fact, an EIC would be in a unique position to measure A_N in $\ell p^\uparrow \to hX$ at $x_F > 0$. In particular $A_N^{\pi^-}$ might allow one to constrain and test the recent extraction of $\hat{H}_{FU}^{h/q,\Im}$ that can play a crucial role in A_N in pp collisions [31], and to discriminate between the GPM and the twist-3 frameworks. In general, further combined theoretical and experimental efforts will help us to deeper understand the underlying QCD mechanism of transverse single-spin asymmetries.

ACKNOWLEDGMENTS

This work is supported by the U.S. Department of Energy under Contract No. DE-FG02-07ER41460 (L. G.), No. DE-AC52-06NA25396 (Z. K.), No. DE-AC05-06OR23177 (A. P.), No. DE-AC02-98CH10886 (D. P.), the National Science Foundation under Grant No. PHY-1205942 (A. M), as well as the LDRD program at LANL (Z. K.) and RIKEN BNL Research Center (D. P.).

[1] D. L. Adams *et al.* (FNAL-E704), Phys. Lett. B **264**, 462 (1991).
[2] S. S. Adler *et al.* (PHENIX Collaboration), Phys. Rev. Lett. **95**, 202001 (2005).
[3] A. Adare *et al.* (PHENIX Collaboration), Phys. Rev. D **90**, 012006 (2014).
[4] A. Adare *et al.* (PHENIX Collaboration), arXiv:1406.3541 [Phys. Rev. D (to be published)].
[5] J. Adams *et al.* (STAR Collaboration), Phys. Rev. Lett. **92**, 171801 (2004).
[6] B. I. Abelev *et al.* (STAR Collaboration), Phys. Rev. Lett. **101**, 222001 (2008).
[7] L. Adamczyk *et al.* (STAR Collaboration), Phys. Rev. D **86**, 051101 (2012).
[8] I. Arsene *et al.* (BRAHMS), Phys. Rev. Lett. **101**, 042001 (2008).
[9] L. Bland *et al.* (AnDY Collaboration), arXiv:1304.1454.
[10] A. V. Efremov and O. V. Teryaev, Sov. J. Nucl. Phys. **36**, 140 (1982).
[11] A. V. Efremov and O. V. Teryaev, Phys. Lett. **150B**, 383 (1985).
[12] J.-W. Qiu and G. Sterman, Phys. Rev. Lett. **67**, 2264 (1991).
[13] J.-W. Qiu and G. Sterman, Nucl. Phys. **B378**, 52 (1992).
[14] J.-W. Qiu and G. Sterman, Phys. Rev. D **59**, 014004 (1998).
[15] C. Kouvaris, J.-W. Qiu, W. Vogelsang, and F. Yuan, Phys. Rev. D **74**, 114013 (2006).
[16] Z.-B. Kang, J.-W. Qiu, W. Vogelsang, and F. Yuan, Phys. Rev. D **83**, 094001 (2011).
[17] M. Anselmino, M. Boglione, and F. Murgia, Phys. Lett. B **362**, 164 (1995).
[18] M. Anselmino and F. Murgia, Phys. Lett. B **442**, 470 (1998).
[19] M. Anselmino, M. Boglione, U. D'Alesio, E. Leader, S. Melis, and F. Murgia, Phys. Rev. D **73**, 014020 (2006).
[20] M. Anselmino, M. Boglione, U. D'Alesio, E. Leader, S. Melis, F. Murgia, and A. Prokudin, Phys. Rev. D **86**, 074032 (2012).
[21] M. Anselmino, M. Boglione, U. D'Alesio, S. Melis, F. Murgia, and A. Prokudin, Phys. Rev. D **88**, 054023 (2013).
[22] Y. Kanazawa and Y. Koike, Phys. Lett. B **478**, 121 (2000).
[23] H. Eguchi, Y. Koike, and K. Tanaka, Nucl. Phys. **B763**, 198 (2007).
[24] Y. Koike and T. Tomita, Phys. Lett. B **675**, 181 (2009).
[25] K. Kanazawa and Y. Koike, Phys. Rev. D **82**, 034009 (2010).
[26] K. Kanazawa and Y. Koike, Phys. Rev. D **83**, 114024 (2011).
[27] H. Beppu, K. Kanazawa, Y. Koike, and S. Yoshida, Phys. Rev. D **89**, 034029 (2014).
[28] Z.-B. Kang, F. Yuan, and J. Zhou, Phys. Lett. B **691**, 243 (2010).
[29] A. Metz, D. Pitonyak, A. Schäfer, M. Schlegel, W. Vogelsang, and J. Zhou, Phys. Rev. D **86**, 094039 (2012).
[30] A. Metz and D. Pitonyak, Phys. Lett. B **723**, 365 (2013).
[31] K. Kanazawa, Y. Koike, A. Metz, and D. Pitonyak, Phys. Rev. D **89**, 111501(R) (2014).
[32] A. Airapetian *et al.* (HERMES Collaboration), Phys. Lett. B **728**, 183 (2014).
[33] K. Allada *et al.* (Jefferson Lab Hall A Collaboration), Phys. Rev. C **89**, 042201 (2014).
[34] D. W. Sivers, Phys. Rev. D **41**, 83 (1990).
[35] D. W. Sivers, Phys. Rev. D **43**, 261 (1991).
[36] Z.-B. Kang, A. Metz, J.-W. Qiu, and J. Zhou, Phys. Rev. D **84**, 034046 (2011).
[37] F. Yuan and J. Zhou, Phys. Rev. Lett. **103**, 052001 (2009).
[38] K. Kanazawa and Y. Koike, Phys. Rev. D **88**, 074022 (2013).
[39] J. C. Collins, Nucl. Phys. **B396**, 161 (1993).
[40] Y. Koike, AIP Conf. Proc. **675**, 449 (2003).
[41] M. Anselmino, M. Boglione, J. Hansson, and F. Murgia, Eur. Phys. J. C **13**, 519 (2000).
[42] M. Anselmino, M. Boglione, U. D'Alesio, S. Melis, F. Murgia, and A. Prokudin, Phys. Rev. D **81**, 034007 (2010).
[43] M. Anselmino, M. Boglione, U. D'Alesio, S. Melis, F. Murgia, and A. Prokudin, Phys. Rev. D **89**, 114026 (2014).
[44] D. Boer, M. Diehl, R. Milner, R. Venugopalan, W. Vogelsang *et al.*, arXiv:1108.1713.
[45] A. Accardi, V. Guzey, A. Prokudin, and C. Weiss, Eur. Phys. J. A **48**, 92 (2012).
[46] A. Accardi, J. Albacete, M. Anselmino, N. Armesto, E. Aschenauer *et al.*, arXiv:1212.1701.
[47] Z.-B. Kang and J.-W. Qiu, Phys. Rev. D **78**, 034005 (2008).
[48] Z.-B. Kang, J.-W. Qiu, W. Vogelsang, and F. Yuan, Phys. Rev. D **78**, 114013 (2008).
[49] J. Zhou, F. Yuan, and Z.-T. Liang, Phys. Rev. D **81**, 054008 (2010).
[50] H. Beppu, Y. Koike, K. Tanaka, and S. Yoshida, Phys. Rev. D **82**, 054005 (2010).
[51] Y. Koike and S. Yoshida, Phys. Rev. D **84**, 014026 (2011).
[52] Z.-T. Liang, A. Metz, D. Pitonyak, A. Schäfer, Y.-K. Song, and Jian Zhou, Phys. Lett. B **712**, 235 (2012).
[53] A. Metz, D. Pitonyak, A. Schaefer, and J. Zhou, Phys. Rev. D **86**, 114020 (2012).
[54] Y. Hatta, K. Kanazawa, and S. Yoshida, Phys. Rev. D **88**, 014037 (2013).
[55] D. Boer, P. J. Mulders, and F. Pijlman, Nucl. Phys. **B667**, 201 (2003).
[56] Z.-B. Kang, B.-W. Xiao, and F. Yuan, Phys. Rev. Lett. **107**, 152002 (2011).
[57] S. M. Aybat, J. C. Collins, J.-W. Qiu, and T. C. Rogers, Phys. Rev. D **85**, 034043 (2012).
[58] A. Bacchetta, U. D'Alesio, M. Diehl, and C. A. Miller, Phys. Rev. D **70**, 117504 (2004).
[59] A. Efremov, K. Goeke, S. Menzel, A. Metz, and P. Schweitzer, Phys. Lett. B **612**, 233 (2005).
[60] M. Anselmino, M. Boglione, U. D'Alesio, A. Kotzinian, F. Murgia, and A. Prokudin, Phys. Rev. D **72**, 094007 (2005).
[61] W. Vogelsang and F. Yuan, Phys. Rev. D **72**, 054028 (2005).
[62] J. Collins, A. Efremov, K. Goeke, S. Menzel, A. Metz, and P. Schweitzer, Phys. Rev. D **73**, 014021 (2006).
[63] A. Efremov, K. Goeke, and P. Schweitzer, Phys. Rev. D **73**, 094025 (2006).
[64] M. Anselmino, M. Boglione, U. D'Alesio, A. Kotzinian, F. Murgia, A. Prokudin, and C. Türk, Phys. Rev. D **75**, 054032 (2007).
[65] S. Arnold, A. Efremov, K. Goeke, M. Schlegel, and P. Schweitzer, arXiv:0805.2137.
[66] M. Anselmino, M. Boglione, U. D'Alesio, A. Kotzinian, S. Melis, F. Murgia, A. Prokudin, and C. Türk, Eur. Phys. J. A **39**, 89 (2009).

[67] M. Anselmino, M. Boglione, U. D'Alesio, S. Melis, F. Murgia, and A. Prokudin, Phys. Rev. D **87**, 094019 (2013).
[68] P. Sun and F. Yuan, Phys. Rev. D **88**, 114012 (2013).
[69] M. G. Echevarria, A. Idilbi, Z.-B. Kang, and I. Vitev, Phys. Rev. D **89**, 074013 (2014).
[70] Z.-B. Kang, X. Liu, and S. Mantry, Phys. Rev. D **90**, 014041 (2014).
[71] M. Glueck, E. Reya, and A. Vogt, Eur. Phys. J. C **5**, 461 (1998).
[72] D. de Florian, R. Sassot, and M. Stratmann, Phys. Rev. D **75**, 114010 (2007).
[73] Z.-B. Kang and J.-W. Qiu, Phys. Rev. D **79**, 016003 (2009).
[74] J. Zhou, F. Yuan, and Z.-T. Liang, Phys. Rev. D **79**, 114022 (2009).
[75] W. Vogelsang and F. Yuan, Phys. Rev. D **79**, 094010 (2009).
[76] V. Braun, A. Manashov, and B. Pirnay, Phys. Rev. D **80**, 114002 (2009).
[77] Z.-B. Kang, Phys. Rev. D **83**, 036006 (2011).
[78] A. Schaefer and J. Zhou, Phys. Rev. D **85**, 117501 (2012).
[79] J. Ma and Q. Wang, Phys. Lett. B **715**, 157 (2012).
[80] Z.-B. Kang and J.-W. Qiu, Phys. Lett. B **713**, 273 (2012).
[81] J. Ma, Q. Wang, and G. Zhang, Phys. Lett. B **718**, 1358 (2013).
[82] A. Schaefer and J. Zhou, arXiv:1308.4961.
[83] J. Dudek, R. Ent, R. Essig, K. Kumar, C. Meyer *et al.*, Eur. Phys. J. A **48**, 187 (2012).
[84] U. D'Alesio and F. Murgia, Phys. Rev. D **70**, 074009 (2004).
[85] X.-N. Wang, Phys. Rev. C **61**, 064910 (2000).
[86] Y. Zhang, G. I. Fai, G. Papp, G. G. Barnafoldi, and P. Levai, Phys. Rev. C **65**, 034903 (2002).
[87] A. Bacchetta, D. Boer, M. Diehl, and P. J. Mulders, J. High Energy Phys. 08 (2008) 023.
[88] L. Gamberg and Z.-B. Kang, Phys. Lett. B **696**, 109 (2011).
[89] J. C. Collins, Phys. Lett. B **536**, 43 (2002).